K. Oshima, F. Topputo, T. Yanao
Low-Energy Transfers to the Moon with Long Transfer Time
Celestial Mechanics and Dynamical Astronomy, Vol. 131, N. 1, Article 4, 2019, p. 1-19
doi:10.1007/s10569-019-9883-7

Celestial Mechanics and Dynamical Astronomy manuscript No.
(will be inserted by the editor)

Low-Energy Transfers to the Moon with Long Transfer Time

Kenta Oshima · Francesco Topputo · Tomohiro Yanao

Received: date / Accepted: date

Abstract This paper globally explores two-impulse, low-energy Earth–Moon transfers in the planar bicircular restricted four-body problem with transfer time of up to 200 days. A grid search combined with a direct transcription and multiple shooting technique reveals numerous families of optimal low-energy solutions, including some that have not been reported yet. We investigate characteristics of solutions in terms of parameters in two- and three-body dynamics, and discuss a trade-off between cost and transfer time based on Pareto-optimal solutions, with and without lunar gravity assists. Analysis of orbital characteristics reveals the role of the Sun, the Earth, and the Moon in the transfer dynamics.

Keywords Low-energy transfer · Restricted four-body problem · Direct transcription and multiple shooting · Pareto-optimal solution · Lunar gravity assist

1 Introduction

Low-energy transfers to the Moon have remarkable benefits such as a lower cost (Δv) and a wider launch window as compared with the conventional Hohmann transfer (Belbruno 1987; Yamakawa 1993; Belbruno and Miller 1993; Circi and Teofilatto 2001; Perozzi and Di Salvo 2008; Mingotti and Topputo 2011; Topputo 2013; Parker et al. 2013; Parker and Anderson 2013). Because of these advantages, HITEN (Uesugi et al. 1991; Kawaguchi et

K. Oshima
Postdoctoral Research Fellow
National Astronomical Observatory of Japan, Tokyo, 181-8588, Japan
E-mail: kenta.oshima@nao.ac.jp

F. Topputo
Assistant Professor
Department of Aerospace Science and Technology
Politecnico di Milano, 20156, Milano, Italy
E-mail: francesco.topputo@polimi.it

T. Yanao
Professor
Department of Applied Mechanics and Aerospace Engineering
Waseda University, Tokyo, 169-8555, Japan
E-mail: yanao@waseda.jp

al. 1995; Uesugi 1996) and GRAIL (Hoffman 2009; Roncoli and Fujii 2010; Chung et al. 2010; Hatch et al. 2010) adopted low-energy transfers to reach the Moon in spite of a longer transfer time (Δt).

Recently, Topputo (2013) globally explored a (Δt, Δv) solution plane of two-impulse transfers to the Moon lasting up to 100 days, including low-energy transfers. As shown in Figure 1, the solutions cover a wide area of the search space, and intercept many known solutions in previous studies near the local Δv-minima. Some solutions were novel transfers to the Moon, and one of these was later analyzed by Oshima et al. (2017a). Table 1 summarizes the solutions in Figure 1 (the reader can find many of them in Topputo (2013)).

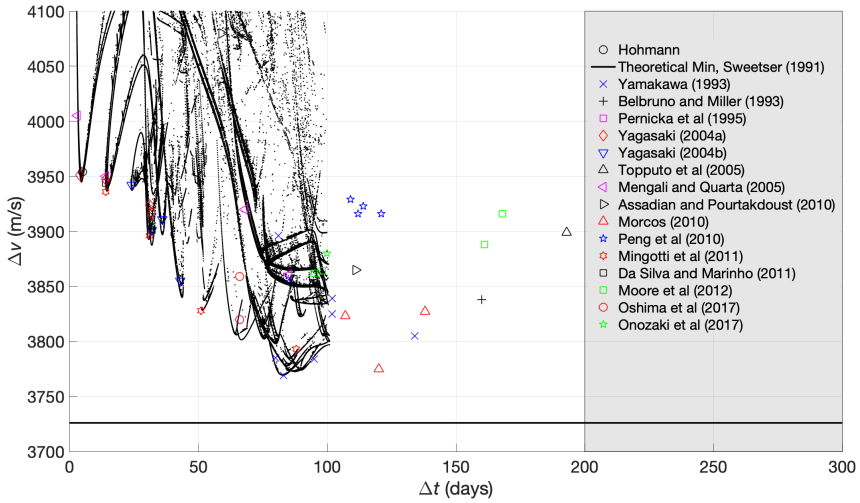

Fig. 1 Solution samples from previous studies (markers) and solutions obtained in Topputo (2013) (black dots) in the (Δt, Δv) plane. See Table 1 for more details of each solution.

Following two previous works (Topputo 2013; Oshima et al. 2017a), this paper globally explores two-impulse, low-energy transfers to the Moon with transfer times up to 200 days. This extension in terms of transfer time aims for a more complete picture of solution structures, but causes computational difficulties. Therefore, our strategy is to firstly perform an extensive grid search to obtain good initial guesses. Then, we optimize these guesses via a direct transcription and multiple shooting technique (Enright and Conway 1992; Betts 1998; Topputo 2013) implementing analytic gradients and the parallel computation.

The obtained solutions cover a wide range of the (Δt, Δv) plane, the large part of which has not been fully explored yet. New solution families result in lower Δv than known solutions. We investigate characteristics of solutions in terms of angular momentum, Kepler energy, and Jacobi energy. We highlight Pareto-optimal solutions to elaborate on a trade-off between Δt and Δv, with and without lunar gravity assists. Analysis of sample Pareto-optimal solutions reveals the role of the Sun, the Earth, and the Moon in reducing the Δv.

The structure of this paper is as follows. Section 2 summarizes the mathematical model. Section 3 introduces the problem statement. Section 4 describes methodologies of the global search. Section 5 shows the computational results. Section 6 presents and analyzes the obtained solutions.

Table 1 Solutions from an initial circular Earth orbit of altitude $h_i = 167$ km to a final circular Moon orbit of altitude $h_f = 100$ km. The fifth column represents the type of transfers (I: Interior, E: Exterior, LGA: Lunar gravity assist).
$^{(\diamond)}$ The theoretical minimum Δv is calculated based on the differences between the Jacobi energy at L_1 and the departure and arrival orbits.
$^{(\dagger)}$ Δv of 676 m/s is added to achieve a 100 km circular Moon orbit.
$^{(*)}$ Δv has been corrected to match the initial and final orbits altitude. The procedure developed is detailed in Appendix 1.

Reference	Δv [m/s]	Δt [days]	Model	Type
Hohmann	3954	5		I
Sweetser (1991)$^{(\diamond)}$	3726	–	Restricted three-body, 2D	I
Yamakawa (1993)$^{(\dagger),(*)}$	3839	102	Bicircular restricted four-body, 2D	E
	3825	102		E
	3896	81		E+LGA
	3785	80		E+LGA
	3805	134		E+LGA
	3769	83		E+LGA
	3784	95		E+LGA
	3856	85		E+LGA
Belbruno and Miller (1993)	3838	160	Full ephemeris n-body, 3D	E+LGA
Pernicka et al. (1995)	3824	292	Restricted three-body, 2D	I
Yagasaki (2004a)	3916	32	Restricted three-body, 2D	E
	3924	31		I
	3947	14		I
	3951	4		I
Yagasaki (2004b)	3855	43	Bicircular restricted four-body, 2D	E+LGA
	3901	32		E
	3911	36		E+LGA
	3942	24		I
Topputo et al. (2005)	3894	255	Restricted three-body, 2D	I
	3899	193		I
Mengali and Quarta (2005)	3861	85	Restricted three-body, 2D	I
	3920	68		I
	3950	14		I
	4005	3		I
Assadian and Pourtakdoust (2010)	3865	111	Bicircular restricted four-body, 3D	E
	3880	96		E
	4080	59		E
Morcos (2010)$^{(*)}$	3823	107	Bicircular restricted four-body, 2D	E+LGA
	3827	138		E+LGA
	3775	120		E+LGA
Peng et al. (2010)$^{(*)}$	3916	112	Patched restricted three-body, 2D	E
	3916	121		E
	3923	114		E
	3929	109		E
Mingotti and Topputo (2011)	3793	88	Bicircular restricted four-body, 2D	E+LGA
	3828	51		E
	3896	31		I
	3936	14		I
Moore et al. (2012)$^{(*)}$	3916	168	Bicircular restricted four-body, 2D	E
	3888	161		E
	3864	98		E
	3862	95		E
Oshima et al. (2017a)	3820	66	Bicircular restricted four-body, 2D	E+LFB
	3859	66		E+LFB
Onozaki et al. (2017)	3880	100	Bicircular restricted four-body, 2D	E

2 Planar Bicircular Restricted Four-Body Problem

The planar bicircular restricted four-body problem (PBRFBP) is considered. The PBRFBP models the motion of a massless particle, P_3, under the gravitational influences of three massive bodies, P_0 (the Sun), P_1 (the Earth), P_2 (the Moon) of masses m_0, m_1, m_2 ($m_0 > m_1 > m_2$), respectively. The model assumes that P_1 and P_2 revolve in circular orbits around their barycenter, P_0 revolves in a circular orbit around the P_1–P_2 barycenter in the same orbital plane as P_1 and P_2, and P_3 moves in the same orbital plane as the massive bodies. In this study, P_0 is the Sun, P_1 is the Earth, and P_2 is the Moon. Let $\boldsymbol{x} := [\boldsymbol{r}, \boldsymbol{v}]^\top$ be the system state, $\boldsymbol{r}$ and $\boldsymbol{v}$ being the position (x, y) and the velocity $(\dot{x}, \dot{y})$ of the particle, respectively. The equations of motion are

$$\dot{\boldsymbol{x}} = \boldsymbol{f}(\boldsymbol{x}, t), \tag{1}$$

where the time-dependent (t) vector field is

$$\boldsymbol{f}(\boldsymbol{x}, t) := \begin{bmatrix} \boldsymbol{v} \\ \boldsymbol{g}(\boldsymbol{r}, t) + \boldsymbol{h}(\boldsymbol{v}) \end{bmatrix}, \tag{2}$$

with

$$\boldsymbol{g}(\boldsymbol{r}, t) := \begin{bmatrix} \partial\Omega_4/\partial x \\ \partial\Omega_4/\partial y \end{bmatrix}, \qquad \boldsymbol{h}(\boldsymbol{v}) := \begin{bmatrix} 2\dot{y} \\ -2\dot{x} \end{bmatrix}, \tag{3}$$

and

$$\Omega_4(x, y, t) := \Omega_3(x, y) + \frac{\mu_s}{\sqrt{(x - a_s\cos\theta_s)^2 + (y - a_s\sin\theta_s)^2}} - \frac{\mu_s}{a_s^2}(x\cos\theta_s + y\sin\theta_s), \tag{4}$$

$$\Omega_3(x, y) := \frac{1}{2}(x^2 + y^2) + \frac{1-\mu}{\sqrt{(x+\mu)^2 + y^2}} + \frac{\mu}{\sqrt{(x-1+\mu)^2 + y^2}} + \frac{1}{2}\mu(1-\mu). \tag{5}$$

In Eqs. (4)–(5), $\mu := m_2/(m_1 + m_2)$, μ_s is the mass of the Sun, a_s is the distance from the Earth–Moon barycenter to the Sun, and $\theta_s(t) := \theta_{s,0} + \omega_s t$ is the phase angle of the Sun for some initial $\theta_{s,0}$ at $t = 0$, while ω_s is the relative angular velocity of the Sun. All the physical parameters used in this paper are in accordance with those in Table 3 in Topputo (2013).

Due to solar perturbation, the Jacobi energy of the circular restricted three-body problem (Szebehely 1967)

$$C := 2\Omega_3 - (\dot{x}^2 + \dot{y}^2). \tag{6}$$

is no longer a constant of motion in the PBRFBP.

The state transition matrix (STM) is defined by using the flow of the system (1)

$$\varphi(\boldsymbol{x}_i, t_i, t_f) := \boldsymbol{x}_i + \int_{t_i}^{t_f} \boldsymbol{f}(\boldsymbol{x}, \tau)\,\mathrm{d}\tau \tag{7}$$

as $\Phi(\boldsymbol{x}, t_i, t_f) := \mathrm{d}\boldsymbol{\varphi}(\boldsymbol{x}, t_i, t_f)/\mathrm{d}\boldsymbol{x}$, and its time evolution is (Topputo 2016)

$$\dot{\Phi}(\boldsymbol{x}, t_i, t) = D_{\boldsymbol{x}}\boldsymbol{f}\,\Phi(\boldsymbol{x}, t_i, t), \quad \Phi(\boldsymbol{x}, t_i, t_i) = I_4, \tag{8}$$

where the subscripts i and f represent initial and final values, respectively, I_4 is a 4×4 identity matrix, and

$$D_{\boldsymbol{x}}\boldsymbol{f} = \begin{bmatrix} 0 & 0 & 1 & 0 \\ 0 & 0 & 0 & 1 \\ \Omega_{4xx} & \Omega_{4xy} & 0 & 2 \\ \Omega_{4yx} & \Omega_{4yy} & -2 & 0 \end{bmatrix}, \tag{9}$$

where the subscripts in Ω_4 indicate partial derivatives.

3 Problem Statement

This study computes two-impulse transfers from an initial circular Earth orbit of altitude $h_i = 167$ km to a final circular Moon orbit of altitude $h_f = 100$ km in the PBRFBP. Since many of the previous studies used these initial and final orbits (see Table 1), we assume these orbits as well for the sake of comparison. The first impulse of magnitude Δv_i at the initial time t_i injects the spacecraft into a trans-lunar trajectory, and the second impulse of magnitude Δv_f at the final time t_f inserts the spacecraft into the final Moon orbit. We set both maneuvers tangential to the local velocities of the initial and final circular orbits. Therefore,

$$\Delta v_i = \sqrt{(\dot{x}_i - y_i)^2 + (\dot{y}_i + x_i + \mu)^2} - \sqrt{\frac{1-\mu}{r_i}}, \tag{10}$$

$$\Delta v_f = \sqrt{(\dot{x}_f - y_f)^2 + (\dot{y}_f + x_f + \mu - 1)^2} - \sqrt{\frac{\mu}{r_f}}, \tag{11}$$

where r_i and r_f are non-dimensional distances from the center of the Earth and the Moon, respectively. Note that $(\dot{x}_i, \dot{y}_i)$ are velocities after the first impulse, and $(\dot{x}_f, \dot{y}_f)$ are those before the second impulse. Therefore, the cost of transfer is $\Delta v = \Delta v_i + \Delta v_f$ and the transfer time is $\Delta t = t_f - t_i$. The following boundary conditions must hold:

$$\boldsymbol{\psi_i} := \begin{bmatrix} (x_i + \mu)^2 + y_i^2 - r_i^2 \\ (x_i + \mu)(\dot{x}_i - y_i) + y_i(\dot{y}_i + x_i + \mu) \end{bmatrix} = \mathbf{0}, \tag{12}$$

$$\boldsymbol{\psi_f} := \begin{bmatrix} (x_f + \mu - 1)^2 + y_f^2 - r_f^2 \\ (x_f + \mu - 1)(\dot{x}_f - y_f) + y_f(\dot{y}_f + x_f + \mu - 1) \end{bmatrix} = \mathbf{0}. \tag{13}$$

See Topputo (2013) for more details on the problem formulation.

4 Methodology

4.1 Generation of Initial Guesses

We compute initial guess solutions by adopting a grid search in the three-dimensional α, β, $\theta_{s,0}$ parameter space; α is an angle between the Earth–Moon line and the line segment from the Earth to the initial position of the spacecraft; β is a proportionality factor of the initial velocity v_i of the spacecraft with respect to the local circular velocity $\sqrt{(1-\mu)/r_i}$, that is, $v_i := \beta\sqrt{(1-\mu)/r_i}$; $\theta_{s,0}$ is the initial phase of the Sun with respect to the Earth–Moon line. Thus, the initial state of the spacecraft in the Earth–Moon rotating frame reads

$$x_i = r_i \cos\alpha - \mu, \quad y_i = r_i \sin\alpha, \quad \dot{x}_i = -(v_i - r_i)\sin\alpha, \quad \dot{y}_i = (v_i - r_i)\cos\alpha. \tag{14}$$

Table 2 summarizes the search space and corresponding number of grid points. Note that each combination of the three parameters uniquely determines an initial condition. This is integrated forward and if the trajectory reaches less than 100 km altitude from the Moon, we label this initial guess "type I" (IG1) and finish the propagation. Otherwise, if a trajectory reaches less than 10,000 km altitude from the Moon, we label it "type II" (IG2) and continue the propagation. We stop the propagation if transfer time reaches 200 days.

Since the grid search produces a huge amount of initial guesses, we optimize only those satisfying the following conditions, which could result in convenient low-energy transfers:

- For IG1: $\Delta v_i \leq 3200$ m/s and $C_f \geq 3.1$
- For IG2: $\Delta v_i \leq 3140$ m/s and $C_f \geq 3.05$

Table 2 Grid search bounds and discretization.

Parameter	Minimum	Maximum	Number of points
α	0	2π	373
β	1.4	$\sqrt{2}$	500
$\theta_{s,0}$	0	2π	500

4.2 Optimization

4.2.1 Direct Transcription and Multiple Shooting

The initial guesses obtained in Section 4.1 are optimized by a direct transcription and multiple shooting technique (Enright and Conway 1992; Betts 1998; Topputo 2013), which translates an optimal control problem into a nonlinear programming (NLP) problem. We divide a trajectory into $N-1$ segments by N nodes evenly spaced in time. Splitting a trajectory reduces the sensitivity and increases the robustness for convergence, which is desirable when aiming to find long-lasting trajectories in a highly sensitive dynamics. For recent applications of the multiple shooting method to optimize chaotic trajectories in multi–body problems, see Whitley and Ocampo (2009); Lantoine et al. (2011) for example. The formulations below closely follow the work in Topputo (2013).

We introduce the NLP variables

$$\boldsymbol{y} \coloneqq \{\boldsymbol{x}_j, t_1, t_N\}, \qquad j = 1, \ldots, N, \tag{15}$$

where $t_1 \coloneqq t_i$ and $t_N \coloneqq t_f$ are initial and final times, respectively, and $\boldsymbol{x}_j \coloneqq (x_j, y_j, \dot{x}_j, \dot{y}_j)$ is the state on the j-th node at time $t_j = t_1 + (t_N - t_1)(j-1)/(N-1)$.

The objective function is given by

$$J(\boldsymbol{y}) \coloneqq \Delta v_1 + \Delta v_N, \tag{16}$$

where $\Delta v_1 \coloneqq \Delta v_i$ and $\Delta v_N \coloneqq \Delta v_f$ are initial and final maneuvers, respectively,

The boundary conditions in terms of the distances from the Earth and the Moon, and the tangency of the maneuvers with the local circular velocities (see Section 3) are given by

$$\boldsymbol{\psi_1} = \mathbf{0}, \quad \boldsymbol{\psi_N} = \mathbf{0}, \tag{17}$$

where Eqs. (12) and (13) are evaluated at the initial and final nodes, respectively.

The state $\boldsymbol{x}_j$ is integrated in the PBRFBP dynamics (1) for the fixed time span $[t_j, t_{j+1}]$. For the continuity of a trajectory, the defect

$$\boldsymbol{\zeta}_j = \boldsymbol{\varphi}(\boldsymbol{x}_j, t_j, t_{j+1}) - \boldsymbol{x}_{j+1}, \qquad j = 1, \ldots, N-1 \tag{18}$$

must vanish.

To avoid impacts with the Earth or the Moon, we impose inequality conditions at each node

$$\boldsymbol{\eta}_j \coloneqq \begin{bmatrix} {R_e}^2 - (x_j + \mu)^2 - {y_j}^2 \\ {R_m}^2 - (x_j + \mu - 1)^2 - {y_j}^2 \end{bmatrix} < \mathbf{0}, \qquad j = 1, \ldots, N, \tag{19}$$

where R_e and R_m are non-dimensional radii of the Earth and the Moon, respectively. After the convergence, we only save non-impact solutions through the entire trajectories. For the sake of consistency in terms duration, an inequality condition $\tau \coloneqq t_1 - t_N < 0$ is also set.

This study provides analytic derivatives of the objective function and constraints with respect to the NLP variables for fast and accurate computations of optimal solutions. See Appendix 2 for the calculation of the analytic derivatives.

4.2.2 Continuation

Optimal solutions are continued in transfer time for broader exploration of solution structures. To this purpose, we compute optimal solutions of the transfer time $\Delta t' := \Delta t + \delta t$ in each continuation step, where Δt is the transfer time of the optimal solution in the previous step, and δt is the continuation increment ($\delta t > 0$) or decrement ($\delta t < 0$). Each continuation process is started from the local optimum, and ends when the continuation fails or $\Delta v \geq 3950$ m/s.

5 Results

We solve the NLP problems by using the MATLAB's constrained optimization solver "fmincon". A tolerance of 10^{-10} is set for all constraints. The optimization process is computed in parallel in terms of each initial guess, which realizes a linear speedup. Trajectories are integrated by a variable step Runge–Kutta algorithm of orders 7 and 8 with absolute and relative tolerances of 10^{-12}.

Figure 2 shows the obtained solutions (gray dots) by the procedure in Section 4, displayed with solutions in Topputo (2013) (black dots) and the known solutions in the literature. The obtained solutions cover a wide range of the (Δt, Δv) space, the large part of which has not been fully explored yet. The solutions also include the low-Δv region where no solutions in the previous studies have been reported (to the best of our knowledge), though the extension of transfer times up to 200 days does not contribute to drastic reductions in Δv. Most of the solutions result in $\Delta v \leq 3850$ m/s because of our selection of initial guesses (see Section 4.1). The obtained solutions could be useful as a database to efficiently pickup candidate trajectories for future lunar missions.

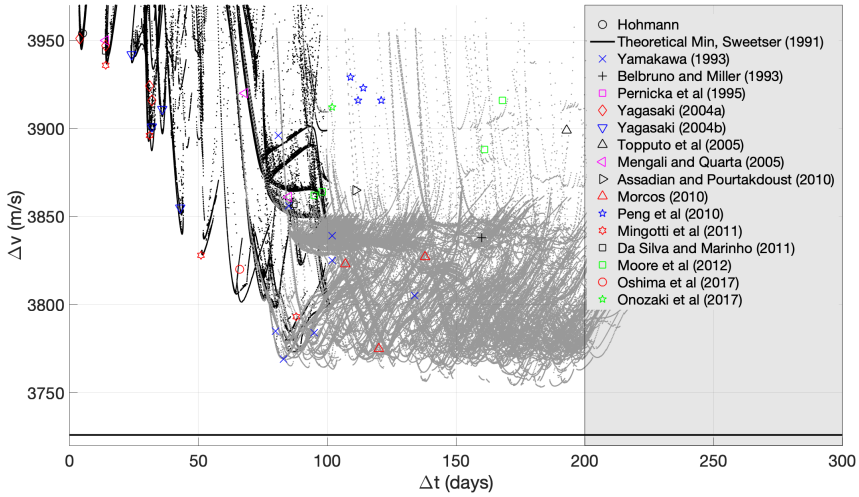

Fig. 2 Obtained solutions by the procedures in Section 4 (gray dots), displayed with solutions in Topputo (2013) (black dots) and the solutions in the previous studies. See Table 1 for more details of the latter.

6 Analysis and Discussion

6.1 Angular Momentum, Kepler Energy, Jacobi Energy

We investigate the final values of the angular momentum around the Moon, h_2, final values of the Kepler energy around the Moon, H_2, initial and final values of the Jacobi energy, C_i and C_f. h_2 and H_2 are given by (Topputo 2013)

$$h_2 = (x + \mu - 1)(\dot{y} + x + \mu - 1) - y(\dot{x} - y), \tag{20}$$

$$H_2 = \frac{1}{2}[(\dot{x} - y)^2 + (\dot{y} + x + \mu - 1)^2] - \frac{\mu}{\sqrt{(x - 1 + \mu)^2 + y^2}}. \tag{21}$$

Figure 3(a) highlights the sign of h_2 at lunar captures. Direct capture solutions ($h_2 > 0$) are shown in blue and retrograde solutions ($h_2 < 0$) are shown in red. From this figure, low-energy solutions tend to end up in direct captures. This is qualitatively understandable from the perspective of dynamical flows around the Lagrange point L_2, where low-energy trajectories guided by stable and unstable manifolds are naturally captured by the Moon in a direct fashion (see Figure 4(b) in Koon et al. (2001) for example). Some retrograde solutions are analyzed in Section 6.2.

Figure 3(b) highlights the sign of H_2 at lunar captures. Ballistic capture solutions ($H_2 < 0$) are shown in red and non-ballistic capture solutions ($H_2 > 0$) are shown in blue. Since our computation focuses on low-energy transfers, most of the obtained solutions are ballistically captured by the Moon.

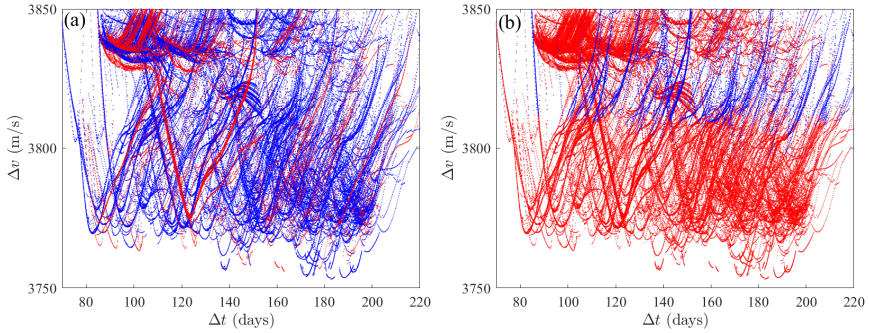

Fig. 3 Solutions classified into positive (blue) and negative (red) values of (a) h_2 and (b) H_2 at final times.

Figure 4 highlights the values of the Jacobi energy at (a) initial time C_i and (b) final time C_f. Since the Jacobi energy directly influences the magnitude of Δv, combinations of high Jacobi energies at initial and final times result in small Δv. Figure 4(b) indicates that in many solutions C_f is sufficiently high considering that the Jacobi energy at $L_2 \approx 3.184$ in the Earth–Moon system. According to Figure 4(a), increasing C_i could still reduce Δv_1 with additional Δt, but the total transfer time may become too long for missions using impulsive maneuvers.

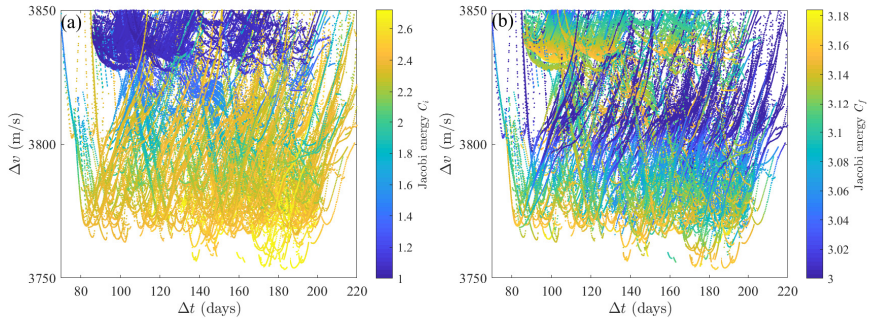

Fig. 4 Solutions colored according to the values of the Jacobi energy at the (a) Earth departure after Δv_i and (b) lunar capture before Δv_f.

6.2 Sample Pareto–Optimal Solutions

This section presents orbital characteristics of sample Pareto–optimal solutions. Figure 5 highlights Pareto–optimal solutions (dark) in terms of Δt and Δv extracted from the obtained solutions (light gray). We only extract those with $\Delta v \leq 3780$ m/s because some Pareto–optimal low-energy solutions were already obtained and analyzed in Topputo (2013). The sample solutions (i)–(iv) are investigated to discuss a trade-off between Δt and Δv.

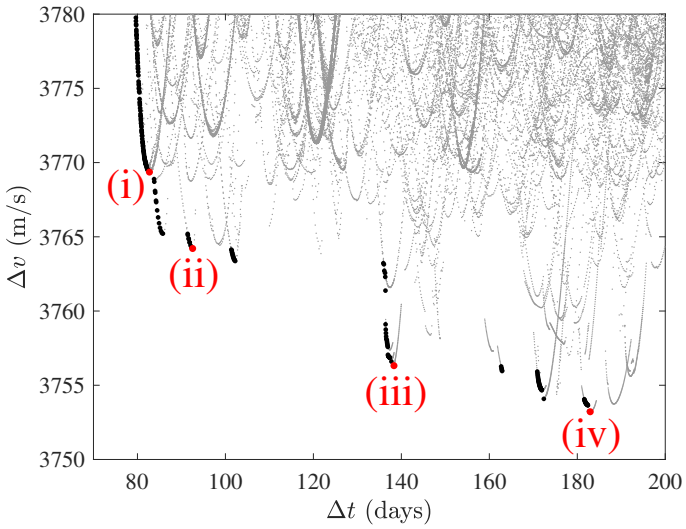

Fig. 5 Pareto–optimal solutions (dark) in terms of Δt and Δv extracted from the obtained solutions (light gray) as those having the optimal balance between Δt and Δv (Topputo 2013). Sample solutions (i)–(iv) (red) are further investigated.

In the remainder, EMrf and SErf abbreviate Earth–Moon and Sun–Earth rotating frames, respectively. In the Earth–Moon rotating frame, the black points indicate the Earth (left) and

the Moon (right), respectively. In the Sun–Earth rotating frame, the black point represents the Earth and the dashed circle indicates the Moon orbit.

6.2.1 Sample (i): (Δt, Δv)=(82.7 days, 3769.4 m/s)

This solution closely coincides with the minimum Δv solution found in Yamakawa (1993); Topputo (2013). In spite of relatively short transfer time among low-energy transfers, it exploits lunar gravity assist (LGA) and solar perturbation effectively as shown in Figure 6 to realize an efficient transfer with a good balance between Δt and Δv.

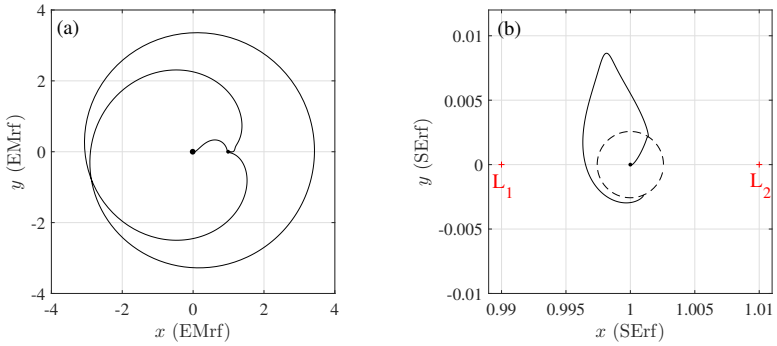

Fig. 6 Trajectories of Sample (i) in the (a) Earth-Moon and (b) Sun-Earth rotating frames.

6.2.2 Sample (ii): (Δt, Δv)=(92.5 days, 3764.2 m/s)

This solution appears to be similar to Sample (i), but having longer Δt and smaller Δv. Unlike ordinary exterior low-energy transfers, the capture mechanism of which can be explained via invariant manifolds around L_2 (Koon et al. 2001), this solution is finally captured from inside of the lunar orbit as shown in Figure 7(b). Figure 7(c) amplifies the vicinity of the Moon in Figure 7(a), where the trajectory bounces in the third quadrant around the Moon in the Earth-Moon rotating frame.

According to the well-known mechanism of the gravity gradient of a perturbative body (Yamakawa 1993; Kawaguchi et al. 1995; Miller 2003), this bounce decreases the angular momentum with respect to the Moon (h_2) by perturbation of the Earth as shown in Figure 7(d). This is an opposite way of exploiting the third-body perturbation to an exterior lunar transfer, in which the solar gravity gradient is used in the second or fourth quadrant to increase the angular momentum with respect to the Earth.

Note that a retrograde capture ($h_2 < 0$) is finally realized in Figure 7(d), which is more favorable than a direct capture in terms of insertion Δv due to the rotational direction of the frame (Campagnola and Russell 2010).

6.2.3 Sample (iii): (Δt, Δv)=(138.3 days, 3756.3 m/s)

As shown in Figure 8(a) and (b), this solution exploits high-altitude lunar flybys with multiple revolutions around the Earth. The high-altitude lunar flybys replenish the small departure

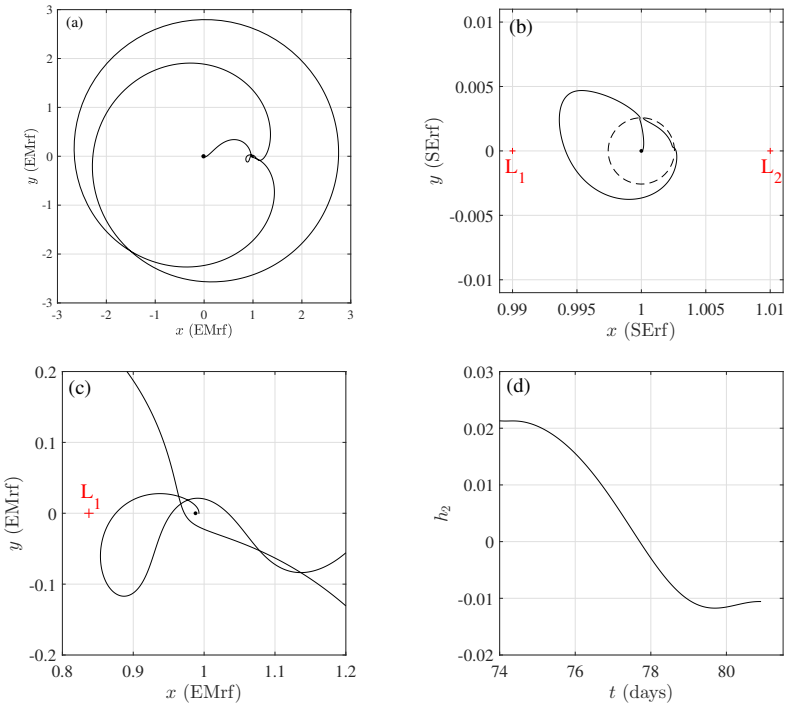

Fig. 7 Trajectories of Sample (ii) in the (a) Earth-Moon and (b) Sun-Earth rotating frames. (c) Amplified figure of (a) around the Moon. (d) Change in h_2 in the final part of the transfer.

Δv_i (high initial Jacobi energy, see Figure 8(c)) by pumping up the semi-major axis a (Ross and Lo 2003; Ross and Scheeres 2007; Topputo et al. 2008; Belbruno et al. 2008; Jerg et al. 2009; Grover and Ross 2009; Campagnola and Russell 2010; Lantoine et al. 2011; Campagnola et al. 2014; Oshima et al. 2017b) as shown in Figure 8(d).

The semi-major axis around the Earth is given by $a = -(1-\mu)/(2H_1)$, where H_1 is the Kepler energy around the Earth. An n:m resonance (n is the number of revolutions of the Moon, and m is the number of revolutions of the spacecraft in the Earth–centered inertial frame) is related to the semi–major axis as $a = (n/m)^{2/3}$.

As a result of increasing the semi-major axis, low-altitude LGA occurs ($t \approx 33$ days) and an effective use of solar perturbation outside the lunar orbit is available to finally realize a low-energy capture by the Moon. This solution exploits dynamics of both inside and outside of the lunar orbit, which may be classified into "interior–exterior" transfers to the Moon.

It is interesting to see Figure 8(d) that from 5 to 30 days, the semi-major axis deviates from 1:2 resonance, though the trajectory is in a fashion of 1:2 resonance and encounters the Moon in one month. This could be due to solar perturbation (Yárnoz et al. 2016) because the Jacobi energy varies to some extent during the revolutions around the Earth even inside the lunar orbit as shown in Figure 8(c).

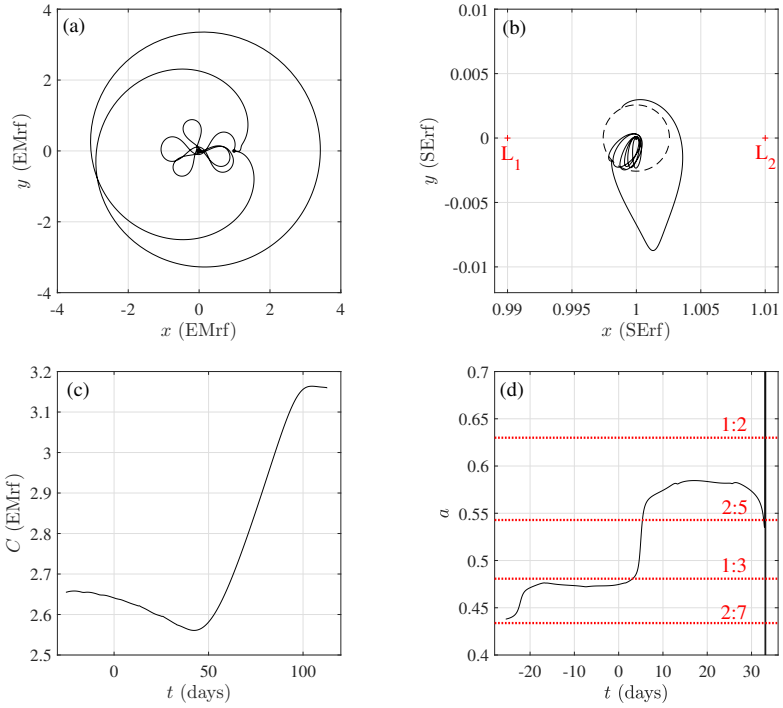

Fig. 8 Trajectories of Sample (iii) in the (a) Earth-Moon and (b) Sun-Earth rotating frames. (c) Change in the Jacobi energy. (d) Change in the semi-major axis around the Earth in the initial part of the transfer.

6.2.4 Sample (iv): (Δt, Δv)=(182.9 days, 3753.2 m/s)

This solution is the minimum Δv solution found in this study. The trajectory can be also classified into the interior–exterior transfer, which exhibits longer Δt and smaller Δv than Sample (iii). In this case, the orbital periods in terms of resonances are consistent according to Figure 9(d); the spacecraft encounters the Moon after 1-month stay in 1:3 resonance and performs the low-altitude LGA ($t \approx 91$ days) after 2-month stay in 2:5 resonance.

6.3 Lunar Gravity Assist

As shown in Section 6.2, LGA plays an important role in Pareto–optimal solutions. Strictly speaking, we detect LGA if the distance from the Moon crosses $1.2 \times r_{\mathrm{SOI}}$ (sphere of influence of the Moon) upward. Note that the threshold $1.2 \times r_{\mathrm{SOI}}$ excludes loops around the Moon before the insertion such as the one in Sample (ii), and the upward condition avoids to detect the lunar capture as LGA.

Figure 10(a) classifies the obtained solutions, combined with the solutions in Topputo (2013), into those using LGA (red) and those not using LGA (blue) based on the above threshold. This figure highlights the quantitative significance of LGA in reducing Δv, which is roughly 100 m/s. Since LGA only requires an Earth departure maneuver to reach the Moon, LGA is useful for reducing Earth departure maneuvers of lunar transfers using solar perturbation outside the lunar orbit.

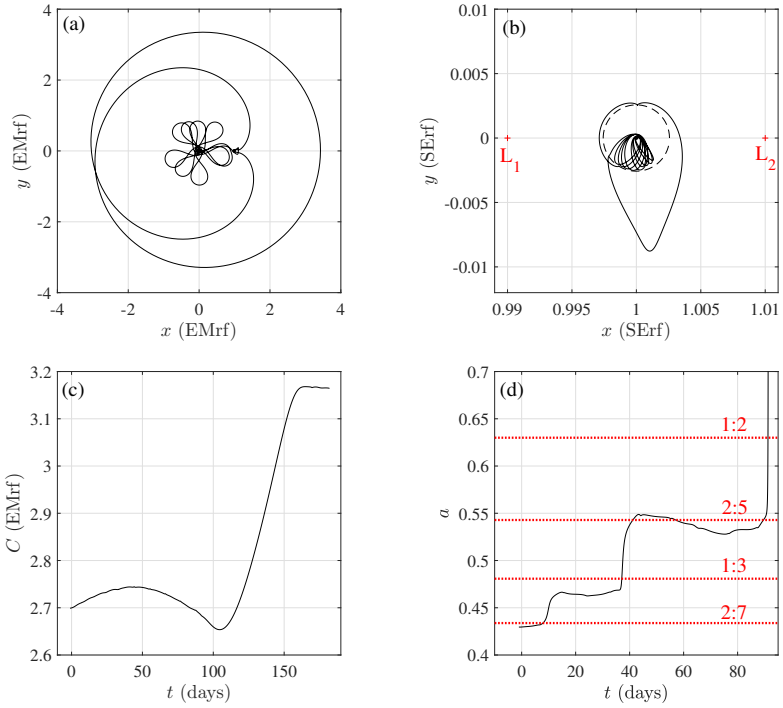

Fig. 9 Trajectories of Sample (iv) in the (a) Earth-Moon and (b) Sun-Earth rotating frames. (c) Change in the Jacobi energy. (d) Change in the semi-major axis around the Earth in the initial part of the transfer.

However, LGA is not always available because of its strict requirements to a launch window. One such example is for a piggyback probe, which usually cannot freely determine its launch date. Because of this reason, we focus on Pareto-optimal solutions among non-LGA trajectories in this section as examples to investigate their orbital characteristics not using LGA.

Figure 10(b) extracts Pareto-optimal solutions (dark) in terms of Δt and Δv among non-LGA solutions (light). Figure 11 presents trajectories of the sample Pareto-optimal solutions (I)–(IV) in the (a) Earth–Moon and (b) Sun–Earth rotating frames. Values of Δt and Δv of each sample are reported in the caption in Figure 11.

Samples (I), (II), and (III) instantly go outside the lunar orbit due to their relatively large departure maneuvers and exploit solar perturbation. Trajectories of Samples (II) and (III) are similar, except that Sample (III) exploits perturbation of the Earth to reduce the angular momentum with respect to the Moon as discussed in Section 6.2. Sample (IV) indeed uses weak LGA. However, it is classified as a non-LGA solution because of our definition of LGA based on the threshold distance from the Moon. Sample (IV) also reduces the angular momentum with respect to the Moon before the insertion.

7 Conclusions

This paper globally explored two-impulse, low-energy Earth-Moon transfers with transfer times up to 200 days in the planar bicircular restricted four-body problem. An extensive

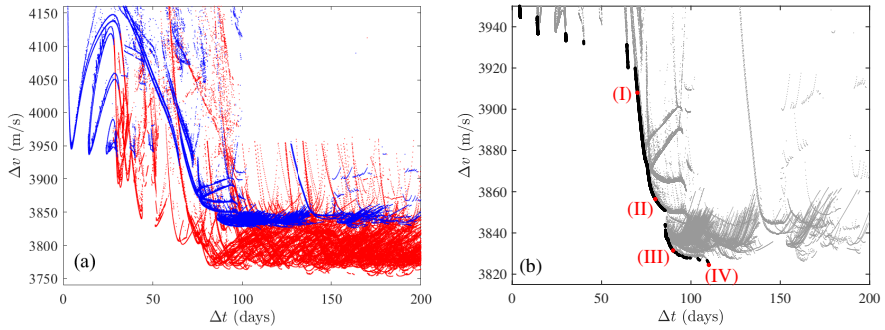

Fig. 10 (a) Solutions in this study and in Topputo (2013), which are classified into those using LGA (red) and those not using LGA (blue). (b) Pareto–optimal solutions (dark) in terms of Δt and Δv extracted from the solutions not using LGA (light). Sample solutions (I)–(IV) (red) are further investigated.

grid search with a direct transcription and multiple shooting technique generated solutions in a wide range of the (Δt, Δv) solution plane. Though the extension of transfer times up to 200 days did not contribute to drastic reductions in Δv, some new families of the obtained solutions resulted in smaller Δv than known solutions. We investigated characteristics of solutions in terms of angular momentum, Kepler energy, and Jacobi energy. We discussed a trade-off between transfer time and fuel expenditure based on Pareto-optimal solutions with or without lunar gravity assists. The maximum gain in Δv of the low-energy transfers was about 200 m/s as compared with a Hohmann transfer, which may be compensated by their much longer transfer times. Still, low-energy lunar transfers are practical options not only for large spacecrafts but also for CubeSats, for which Δv is much higher priority than transfer time. Analyses on orbital characteristics of sample solutions revealed roles of perturbations of the Sun, Earth, and Moon in reducing Δv.

Acknowledgements This study has been partially supported by Grant-in-Aid for JSPS Fellows No. 15J07090, and by JSPS Grant-in-Aid, No. 26800207.

References

Assadian, N., Pourtakdoust, S. H.: Multiobjective genetic optimization of Earth–Moon trajectories in the restricted four-body problem. Adv. Space. Res. **45**, 398–409 (2010). http://dx.doi.org/10.1016/j.asr.2009.10.023

Belbruno, E.: Lunar capture orbits, a method of constructing Earth–Moon trajectories and the lunar GAS mission. In: AIAA Paper 971054, Proceedings of the AIAA/DGLR/JSASS International Electric Propulsion Conference (1987).

Belbruno, E., Miller, J.: Sun-perturbed Earth-to-Moon transfers with ballistic capture. J. Guid. Control Dyn. **16**, 770–775 (1993). doi:10.2514/3.21079

Belbruno, E., Topputo, F., Gidea, M.: Resonance transition associated to weak capture in the restricted three-body problem. Adv. Space. Res. **42**, 18–39 (2008). doi:10.1016/j.asr.2008.01.018

Betts, J. T.: Survey of numerical methods for trajectory optimization. J. Guid. Control Dyn. **21**, 193–207 (1998). http://dx.doi.org/10.2514/2.4231

Campagnola, S., Russell, R. P.: Endgame problem part 2: Multi-body technique and T-P graph. J. Guid. Control Dyn. **33**, 476–486 (2010). doi:10.2514/1.44290

Campagnola, S., Boutonnet, A., Schoenmaekers, J., Grebow, D. J., Petropoulos, A.E.: Tisserand-Leveraging Transfer. J. Guid. Control Dyn. **37**, 1202–1210 (2014). doi:10.2514/1.62369

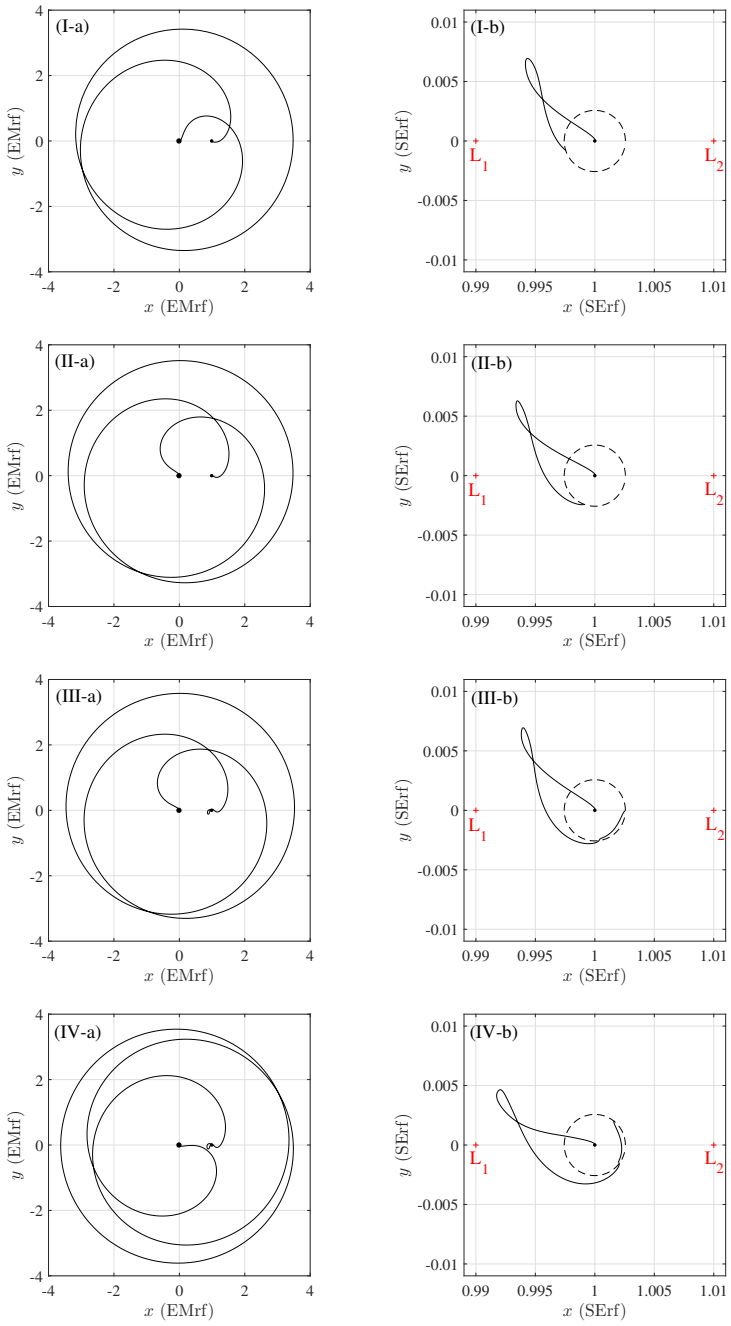

Fig. 11 Trajectories of the sample Pareto–optimal solutions (I)–(IV) in the (a) Earth-Moon and (b) Sun-Earth rotating frames. Sample (I): (Δt, Δv)=(70.0 days, 3908.0 m/s), Sample (II): (Δt, Δv)=(80.1 days, 3856.4 m/s), Sample (III): (Δt, Δv)=(90.0 days, 3831.5 m/s), Sample (IV): (Δt, Δv)=(110.0 days, 3824.5 m/s).

Chung, M. J., Hatch, S. J., Kangas, J. A., Long, S. M., Roncoli, R. B., Sweetser, T. H.: Trans-lunar cruise trajectory design of GRAIL (Gravity Recovery and Interior Laboratory) mission. In Paper AIAA 2010-8384, AIAA Guidance, Navigation, and Control Conference, Toronto, Ontario, Canada, 2-5 August, (2010).

Circi, C., Teofilatto, P.: On the dynamics of weak stability boundary lunar transfers. Celest. Mech. Dyn. Astr. **79**, 41–72 (2001). doi:10.1023/A:1011153610564

Enright, P. J, and Conway, B. A.: Discrete approximations to optimal trajectories using direct transcription and nonlinear programming. J. Guid. Control Dyn. **15**, 994–1002 (1992). http://dx.doi.org/10.2514/3.20934

Grover, P., Ross, S. D.: Designing trajectories in a planet-moon environment using the controlled Keplerian map. J. Guid. Control Dyn. **32**, 437–444 (2009). doi:10.2514/1.38320

Hatch, S. J., Roncoli, R. B., Sweetser, T. H.: Trans-lunar cruise trajectory design of GRAIL (Gravity Recovery and Interior Laboratory) mission. In Paper AIAA 2010-8385, AIAA Guidance, Navigation, and Control Conference, Toronto, Ontario, Canada, 2-5 August, (2010).

Hoffman, T. L.: GRAIL: Gravity Mapping the Moon. In IEEE Aerospace Conference, Big Sky, Montana, 7–14 March (2009).

Jerg, S., Junge, O., Ross, S. D.: Optimal capture trajectories using multiple gravity assists. Commun. Nonlinear Sci. Numer. Simul. **14**, 4168–4175 (2009). doi:10.1016/j.cnsns.2008.12.009

Kawaguchi, J., Yamakawa, H., Uesugi, K., Matsuo, H.: On making use of lunar and solar gravity assists in LUNAR-A, PLANET-B missions. Acta Astronaut. **35**, 633–642 (1995). doi:10.1016/0094-5765(95)00013-p

Koon, W. S., Lo, M. W., Marsden, J. E., Ross, S. D.: Low energy transfer to the Moon. Celest. Mech. Dyn. Astr. **81**, 63–73 (2001). doi:10.1023/A:1013359120468

Lantoine, G., Russell, R. P., Campagnola, S.: Optimization of low-energy resonant hopping transfers between planetary moons. Acta Astronaut. **68**, 1361–1378 (2011). doi:10.1016/j.actaastro.2010.09.021

Mengali, G., Quarta, A.: Optimization of biimpulsive trajectories in the Earth-Moon restricted three-body system. J. Guid. Control Dyn. **28**, 209–216 (2005). http://dx.doi.org/10.2514/1.7702

Miller, J.: Lunar transfer trajectory design and the four-body problem. 13th AAS/AIAA Space Flight Mechanics Meeting, AAS 03-144, At Ponce, Puerto Rico, (2003).

Mingotti, G., Topputo, F.: Ways to the Moon: A survey. 21th AAS/AIAA Space Flight Mechanics Meeting, AAS 11-283, New Orleans, (2011).

Moore, A., Ober-Bl$'$obaum, S., Marsden, J. E.: Trajectory design combining invariant manifolds with discrete mechanics and optimal control. J. Guid. Control Dyn. **35**, 1507–1525 (2012). doi:10.2514/1.55426

Morcos, F. M.: Design and optimization of body-to-body impulsive trajectories in restricted four-body models. Ph. D. dissertation, The University of Texas at Austin (2010).

Onozaki, K., Yoshimura, H., Ross, S. D.: Tube dynamics and low energy Earth-Moon transfers in the 4-body system. Adv. Space. Res. **60**, 2117–2132 (2017). http://dx.doi.org/10.1016/j.asr.2017.07.046

Oshima, K., Topputo, F., Campagnola, S., Yanao, T.: Analysis of medium-energy transfers to the Moon. Celest. Mech. Dyn. Astr. **127**, 285–300 (2017a). doi:10.1007/s10569-016-9727-7

Oshima, K., Campagnola, S., Yanao, T.: Global search for low-thrust transfers to the Moon in the planar circular restricted three-body problem. Celest. Mech. Dyn. Astr. **128**, 303–322 (2017b). doi: 10.1007/s10569-016-9748-2

Parker, J. S., Anderson, R. L., Peterson, A.: Surveying ballistic transfers to low lunar orbit. J. Guid. Control Dyn. **36**, 1501–1511 (2013). http://dx.doi.org/10.2514/1.55661

Parker, J. S., Anderson, R. L.: Targeting low-energy transfers to low lunar orbit. Acta Astronaut. **84**, 1–14 (2013). http://dx.doi.org/10.1016/j.actaastro.2012.10.033

Peng, L., Wang, Y., Dai, G., Chang, Y., Chen, F.: Optimization of the Earth-Moon low energy transfer with differential evolution based on uniform design. IEEE Congress on Evolutionary Computation, Barcelona, (2010). doi:10.1109/CEC.2010.5586384

Pernicka, H. J., Scarberry, D. P., Marsh, S. M., Sweetser, T. H.: A search for low Δv Earth-to-Moon trajectories. J. Astronaut. Sci. **43**, 77–88 (1995).

Perozzi, E., Di Salvo, A.: Novel spaceways for reaching the Moon: An assessment for exploration. Celest. Mech. Dyn. Astr. **102**, 207–218 (2008). doi:10.1007/s10569-008-9156-3

Roncoli, R. B., Fujii, K. K.: Mission design overview for the Gravity Recovery and Interior Laboratory (GRAIL) mission. In Paper AIAA 2010-8383, AIAA Guidance, Navigation, and Control Conference, Toronto, Ontario, Canada, 2-5 August, (2010).

Ross, S. D., Lo, M. W.: Design of a multi-moon orbiter. 13th AAS/AIAA Space Flight Mechanics Meeting, AAS 03-143, At Ponce, Puerto Rico, (2003).

Ross, S. D., Scheeres, D. J.: Multiple gravity assists, capture, and escape in the restricted three-body problem. SIAM J. Appl. Dyn. Syst. **6**, 576–596 (2007). doi:10.1137/060663374

Sweetser, T.H.: An estimate of the global minimum Δv needed for Earth-Moon transfer. Adv. Astronaut. Sci. **75**, 111–120 (1991).
Szebehely, V.: Theory of Orbits: The Restricted Problem of Three Bodies. Academic Press Inc, New York (1967)
Topputo, F.: On optimal two-impulse Earth–Moon transfers in a four-body model. Celest. Mech. Dyn. Astr. **117**, 279–313 (2013). doi:10.1007/s10569-013-9513-8
Topputo, F.: Fast numerical approximation of invariant manifolds in the circular restricted three-body problem. Commun. Nonlinear Sci. Numer. Simul. **32**, 89–98 (2016). doi:10.1016/j.cnsns.2015.08.004
Topputo, F., Belbruno, E., Gidea, M.: Resonant motion, ballistic escape, and their applications in astrodynamics. Adv. Space. Res. **42**, 6–17 (2008). doi:10.1016/j.asr.2008.01.017
Topputo, F., Vasile, M., Bernelli-Zazzera, F.: Earth-to-Moon low energy transfers targeting L_1 hyperbolic transit orbits. Annals of the New York Academy of Sciences **1065**, 55–76 (2005).
Uesugi, K.: Results of the MUSES-A "HITEN" mission. Adv. Space. Res. **18**, 69–72 (1996). doi:10.1016/0273-1177(96)00090-7
Uesugi, K., Matsuo, H., Kawaguchi, J., Hayashi, T.: Japanese first double lunar swingby mission "HITEN". Acta Astronaut. **25**, 347–355 (1991). doi:10.1016/0094-5765(91)90014-v
Whitley, R. J., Ocampo, C. A.: Direct multiple shooting optimization with variable problem parameters. In Proceedings of the 47th AIAA Aerospace Sciences Meeting Including the New Horizons Forum and Aerospace Exposition, Orlando, (2009).
Yagasaki, K.: Computation of low energy Earth-to-Moon transfers with moderate flight time. Physica D. **197**, 313–331 (2004). doi:10.1016/j.physd.2004.07.005
Yagasaki, K.: Sun-perturbed Earth-to-Moon transfers with low energy and moderate flight time. Celest. Mech. Dyn. Astr. **90**, 197–212 (2004). doi:10.1007/s10569-004-0406-8
Yamakawa, H.: On Earth-Moon transfer trajectory with gravitational capture. Ph. D. dissertation, The University of Tokyo (1993).
Yárnoz, D. G., Yam, C. H., Campagnola, S., Kawakatsu, Y.: Extended Tisserand-Poincaré graph and multiple lunar swingby design with Sun perturbation. In Proceedings of the 6th International Conference on Astrodynamics Tools and Techniques (2016).

Appendix 1

Since the majority of the studies in Table 1 use the initial and final circular orbits around the Earth and the Moon of "reference"altitudes 167 km and 100 km, respectively, this study transforms the values of Δv of the solutions using different altitudes (Yamakawa 1993; Morcos 2010; Peng et al. 2010; Moore et al. 2012) for a fair comparison. The following calculation shows the case of transforming Earth departure maneuvers, but the transformation of Moon arrival maneuvers is similar.

The Kepler energy at departure from an initial Earth circular orbit of a different altitude from the reference altitude is

$$H_{E1} = \frac{1}{2}{v_{E1}}^2 - \frac{1-\mu}{r_{E1}}, \tag{22}$$

where v_{E1} and r_{E1} are the magnitude of the spacecraft's velocity in the Earth–centered inertial frame and the distance from the center of the Earth, respectively.

The required velocity v_{E2} to achieve H_{E1} from the reference altitude at the Earth is

$$v_{E2} = \sqrt{2(H_{E1} + \frac{1-\mu}{r_{E2}})}, \tag{23}$$

where r_{E2} is the distance between the reference circular orbit and the center of the Earth.

The transformed Earth departure maneuver can be computed by assuming the tangential maneuver as

$$\Delta v_E = v_{E2} - \sqrt{\frac{1-\mu}{r_{E2}}}. \tag{24}$$

Appendix 2

This appendix presents analytic derivatives of the objective function and the constraints with respect to the NLP variables in the optimization problem in Section 4.2.1. For the sake of simple notations, we assume $N = 4$ in the following expressions, but the generalization is straightforward.

The derivative of the objective function J with respect to the NLP variables $\boldsymbol{y}$ can be expressed as

$$\frac{\partial J}{\partial \boldsymbol{y}} = \begin{bmatrix} P_1 & O & P_N & O \end{bmatrix}, \tag{25}$$

where

$$P_1 \coloneqq \frac{\partial J}{\partial \boldsymbol{x}_1} = \frac{1}{\sqrt{(\dot{x}_1 - y_1)^2 + (\dot{y}_1 + x_1 + \mu)^2}} \begin{bmatrix} \dot{y}_1 + x_1 + \mu & y_1 - \dot{x}_1 & \dot{x}_1 - y_1 & \dot{y}_1 + x_1 + \mu \end{bmatrix}, \tag{26}$$

$$P_N \coloneqq \frac{\partial J}{\partial \boldsymbol{x}_N} = \frac{1}{\sqrt{(\dot{x}_N - y_N)^2 + (\dot{y}_N + x_N + \mu - 1)^2}} \begin{bmatrix} \dot{y}_N + x_N + \mu - 1 & y_N - \dot{x}_N & \dot{x}_N - y_N & \dot{y}_N + x_N + \mu - 1 \end{bmatrix}. \tag{27}$$

The derivative of the equality constraints $\boldsymbol{c} \coloneqq \{\boldsymbol{\zeta}_j, \boldsymbol{\psi}_1, \boldsymbol{\psi}_N\} = \boldsymbol{0}$ with respect to the NLP variables $\boldsymbol{y}$ can be expressed as

$$\frac{\partial \boldsymbol{c}}{\partial \boldsymbol{y}} = \begin{bmatrix} \boldsymbol{\Phi}(t_1, t_2) & -I_4 & O & O & Q_1^1 & Q_N^1 \\ O & \boldsymbol{\Phi}(t_2, t_3) & -I_4 & O & Q_1^2 & Q_N^2 \\ O & O & \boldsymbol{\Phi}(t_{N-1}, t_N) & -I_4 & Q_1^{N-1} & Q_N^{N-1} \\ R_1 & O & O & O & O & O \\ O & O & O & R_N & O & O \end{bmatrix}, \tag{28}$$

where

$$Q_1^j \coloneqq \frac{\partial \boldsymbol{\zeta}_j}{\partial \boldsymbol{t}_1} = -\frac{N-j}{N-1} \boldsymbol{\Phi}(t_j, t_{j+1}) \boldsymbol{f}(\boldsymbol{x}_j, t_j) + \frac{N-j-1}{N-1} \boldsymbol{f}(\boldsymbol{\varphi}(\boldsymbol{x}_j, t_j, t_{j+1}), t_{j+1}), \qquad j = 1, \ldots, N-1, \tag{29}$$

$$Q_N^j \coloneqq \frac{\partial \boldsymbol{\zeta}_j}{\partial \boldsymbol{t}_N} = -\frac{j-1}{N-1} \boldsymbol{\Phi}(t_j, t_{j+1}) \boldsymbol{f}(\boldsymbol{x}_j, t_j) + \frac{j}{N-1} \boldsymbol{f}(\boldsymbol{\varphi}(\boldsymbol{x}_j, t_j, t_{j+1}), t_{j+1}), \qquad j = 1, \ldots, N-1, \tag{30}$$

$$R_1 \coloneqq \frac{\partial \boldsymbol{\psi}_1}{\partial \boldsymbol{x}_1} = \begin{bmatrix} 2(x_1 + \mu) & 2y_1 & 0 & 0 \\ \dot{x}_1 & \dot{y}_1 & x_1 + \mu & y_1 \end{bmatrix}, \tag{31}$$

$$R_N \coloneqq \frac{\partial \boldsymbol{\psi}_N}{\partial \boldsymbol{x}_N} = \begin{bmatrix} 2(x_N + \mu - 1) & 2y_N & 0 & 0 \\ \dot{x}_N & \dot{y}_N & x_N + \mu - 1 & y_N \end{bmatrix}. \tag{32}$$

The derivative of the inequality constraints $\boldsymbol{g}(\boldsymbol{y}) \coloneqq \{\boldsymbol{\eta}_j, \tau\} < \boldsymbol{0}$ with respect to the NLP variables $\boldsymbol{y}$ can be expressed as

$$\frac{\partial \boldsymbol{g}}{\partial \boldsymbol{y}} = \begin{bmatrix} S_1 & O & O & O & O \\ O & S_2 & O & O & O \\ O & O & S_3 & O & O \\ O & O & O & S_N & O \\ O & O & O & O & S_t \end{bmatrix}, \tag{33}$$

where

$$S_j \coloneqq \frac{\partial \boldsymbol{\eta}_j}{\partial \boldsymbol{x}_j} = \begin{bmatrix} -2(x_j+\mu) & -2y_j & 0 & 0 \\ -2(x_j+\mu-1) & -2y_j & 0 & 0 \end{bmatrix}, \qquad j = 1, \ldots, N, \tag{34}$$

$$S_t \coloneqq \begin{bmatrix} \dfrac{\partial \tau}{\partial t_1} & \dfrac{\partial \tau}{\partial t_N} \end{bmatrix} = \begin{bmatrix} 1 & -1 \end{bmatrix}. \tag{35}$$